Infrared-pump–x-ray-probe spectroscopy of vibrationally excited molecules

Nina Ignatova,[1,2,*] Vinícius V. da Cruz,[2] Rafael C. Couto,[2,3] Emilie Ertan,[4] Michael Odelius,[4] Hans Ågren,[1,2] Freddy F. Guimarães,[3] Andrei Zimin,[1,2] Sergey P. Polyutov,[1] Faris Gel'mukhanov,[1,2] and Victor Kimberg[1,2,†]

[1]*Institute of Nanotechnology, Spectroscopy and Quantum Chemistry, Siberian Federal University, 660041 Krasnoyarsk, Russia*

[2]*Theoretical Chemistry and Biology, Royal Institute of Technology, 10691 Stockholm, Sweden*

[3]*Instituto de Química, Universidade Federal de Goiás, Campus Samambaia, CP 131 CEP 74001-970, Goiânia-GO, Brazil*

[4]*Department of Physics, Stockholm University, AlbaNova University Center, 10691 Stockholm, Sweden*

(Received 12 October 2016; revised manuscript received 6 February 2017; published 7 April 2017)

We develop a theory of infrared (IR)-pump–x-ray-probe spectroscopy for molecular studies. We illustrate advantages of the proposed scheme by means of numerical simulations employing a vibrational wave packet technique applied to x-ray absorption and resonant inelastic x-ray scattering (RIXS) spectra of the water molecule vibrationally excited by a preceding IR field. The promotion of the vibrationally excited molecule to the dissociative $1a_1^{-1}4a_1$ and bound $1a_1^{-1}2b_2$ core-excited states with qualitatively different shapes of the potential energy surfaces creates nuclear wave packets localized along and between the OH bonds, respectively. The projection of these wave packets on the final vibrational states, governed by selection and propensity rules, results in spatial selectivity of RIXS sensitive to the initial vibrationally excited state, which makes it possible to probe selectively the ground state properties along different modes. In addition, we propose to use RIXS as a tool to study x-ray absorption from a selected vibrational level of the ground state when the spectral resolution is sufficiently high to resolve vibrational overtones. The proposed technique has potential applications for advanced mapping of multidimensional potential energy surfaces of ground and core-excited molecular states, for symmetry-resolved spectroscopy, and for steering chemical reactions.

DOI: 10.1103/PhysRevA.95.042502

I. INTRODUCTION

Infrared (IR) and x-ray spectroscopy, widely used for molecular studies, each has merits and limitations when applied for a particular purpose. IR spectroscopic techniques make it possible to measure rovibrational levels of the molecular electronic ground state at ultra-high resolution. Numerous techniques have been developed for studies of potential energy surfaces (PESs) in polyatomic systems making use of IR radiation [1,2]. X-rays, which address transitions of core electrons, are widely used to study nuclear dynamics in core-excited, valence-excited, and ground electronic states with the help of x-ray absorption spectroscopy (XAS) and resonant inelastic x-ray scattering (RIXS) [3,4]. High element selectivity of the core orbitals makes x-ray techniques useful for site-selective studies of complex systems. The RIXS scheme can also be successfully applied in advanced studies of molecular ground states, where highly excited vibrational levels are reached in the course of the x-ray scattering to the ground electronic state [5–7]. The ultrafast wide range propagation of the nuclear wave packet in the intermediate core-excited state makes RIXS a powerful tool to investigate the ground state PESs in extended spatial regions. The spectral resolution of RIXS, in general worse than that of the IR spectroscopy, is now drastically improving through technological development. For example, a 1.4 meV (11 cm^{-1}) resolution was recently reached in a nonresonant hard x-ray scattering experiment [8]. One can expect that the presently available overall resolution of about 75 meV near the O 1s edge [7] will be improved down to a few meVs in the nearest future. RIXS can compete with IR spectroscopy in studies of liquids where the IR spectral resolution becomes worse due to environmental broadening. One should also mention here that the intensity distribution of vibrational resonances in RIXS differs strongly from IR spectroscopy due to the qualitatively different transition matrix elements and, hence, different selection rules [9]. This makes the RIXS technique an efficacious complementary method to IR spectroscopy in studies of molecular vibrations.

The conventional RIXS process starts from the lowest vibrational level. The present paper is devoted to a technique which combines subsequent IR and x-ray excitations of a molecule. The pump-probe method discussed here is a two-step method. First, the molecule is prepared by an IR pulse which creates a population of the excited vibrational levels in the electronic ground state. At the second step, the vibrationally excited molecule is probed with x rays using the XAS and RIXS schemes. A similar technique was discussed previously in terms of phase-sensitive x-ray absorption driven by strong IR fields, when a coherent superposition of vibrational states, the nuclear wave packet, is created and its dynamics in the electronic ground state is probed by means of XAS [10–12]. In contrast, in this work we study changes in XAS and RIXS spectra when the process starts from a single excited vibrational state. The state-selective vibrational excitation can be reached using the stimulated Raman process with two coherent IR pulses [13–15] or with the help of specially prepared strong $\sin^2$-shaped laser pulses [16].

As a proof-of-principle theoretical study, we focus here on a rather simple system, gas phase water, in order to show advantages of vibrationally preconditioned x-ray spectroscopy for symmetry and Franck-Condon control of vibrational excitation by choosing a proper initial vibrationally excited state. The RIXS process in vibrationally excited molecules leading back to the ground electronic state provides an efficient

*ninai@kth.se
†kimberg@kth.se

tool to study the ground state properties complementary to IR spectroscopy. The IR-pump–x-ray-probe technique can be adapted for studies of rather complex systems, for example, as an additional tool reinforcing existing attempts of probing the local structure of liquid water, or for an advanced control over the nuclear dynamics of chemical reactions.

The paper is organized as follows. In Sec. II we present the theoretical approach employed in the *ab initio* electronic structure calculations and in the nuclear wave packet simulations. In Sec. III we discuss our results for XAS (Secs. III A and III C) and RIXS (Sec. III B) of vibrationally excited molecules. Our findings are summarized in Sec. IV.

II. THEORY

The studied gas phase water molecule has three vibrational degrees of freedom: symmetric and antisymmetric stretching and bending modes with vibrational quanta $\omega_s = 0.4531$ eV, $\omega_a = 0.4654$ eV, and $\omega_b = 0.1976$ eV, respectively [17]. In the ground electronic state, the two stretching modes are nearly degenerate and strongly coupled due to the close vibrational frequencies and anharmonicity (Darling-Dennison coupling) [18,19] and have to be considered together for a proper system description [20,21]. There is also a coupling between bending and the symmetric stretching modes observed by a Fermi resonance [18], which, however, is much weaker compared to the strong Darling-Dennison coupling of the stretching modes. Moreover, the bending mode excitation is very weak in XAS and RIXS spectra of the two lowest core-excited states of water, considered in the present paper, as has been shown by recent experiments [5,7,22]. These conditions make it possible to use a rather good approximation of neglecting the bending motion and to focus fully on the two coupled stretching modes using a two-dimensional (2D) approach, as described below. Furthermore, the 2D approach allows one to avoid complexity and to present the physical picture more clearly.

In the present work we study the water molecule with two-step pump-probe spectroscopy: (1) an IR pulse populates a particular vibrational level of the electronic ground state and (2) the following x-ray photon promotes an oxygen 1s electron to the LUMO $4a_1$ and LUMO+1 $2b_2$ molecular orbitals. For brevity, the corresponding core-excited states $|O1s^{-1}4a_1^1\rangle$ and $|O1s^{-1}2b_2^1\rangle$ are denoted as $4a_1$ and $2b_2$, respectively. We focus here on investigations of the XAS and RIXS spectra when the initial vibrational state of the water molecule is prepared by a preceding IR pulse.

A. 2D approach for coupled stretching modes

For the coupled stretching modes [Fig. 1(a)], the 2D vibrational wave functions can be assigned as $\psi_v = \psi_{sa}$, where the indices s,a describe the symmetric and antisymmetric vibrational excited quantum $v = (sa)$. The initial vibrational excitation can be achieved with the help of an IR field resonant to the vibrational transition in the ground electronic state. When the IR field is weak only the first vibrational levels (10) and (01) are populated. The higher vibrational levels are populated by a ladder-type process when the intensity of the IR laser is sufficiently high. The strength of each IR transition is defined by the **R** dependence of the permanent dipole moment

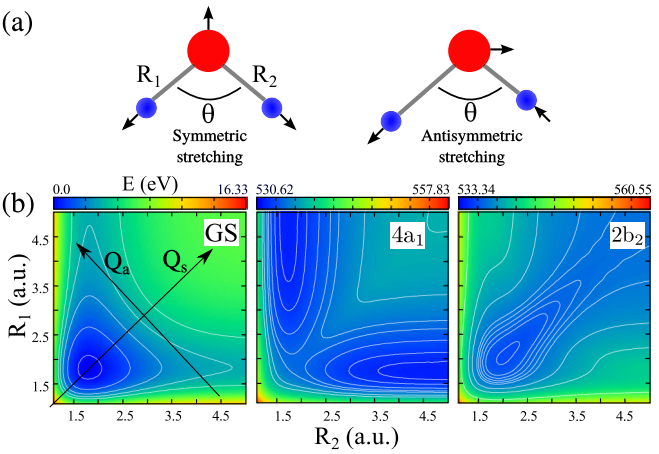

FIG. 1. (a) The stretching vibrational modes of the water molecule and valence coordinates representation. (b) 2D stretching mode potential energy surfaces of the ground state (GS) and two lowest core-excited states of water molecule (dissociative $4a_1$ and bound $2b_2$) in valence coordinates R_1, R_2 in atomic units. The directions of the normal symmetric Q_s and antisymmetric Q_a modes are also shown schematically.

d in the ground electronic state

$$d'_{Q_s}\langle\psi_{sa}|Q_s|\psi_{(s\pm1)a}\rangle, \quad d'_{Q_a}\langle\psi_{sa}|Q_a|\psi_{s(a\pm1)}\rangle, \tag{1}$$

where $d'_{Q_{s,a}}$ is the derivative of the dipole moment over the normal coordinate $Q_{s,a}$ at the equilibrium geometry. One should notice that the vibrational levels in the ground electronic state of H_2O show grouping according to the group number $n = s + a$. Each nth group consists of $n + 1$ close-lying vibrational levels [7,9,20].

The PESs for the ground and the two lowest $4a_1$ [23,24] and $2b_2$ [24] core-excited states were computed at the RASPT2 theory level [25] implemented in the MOLCAS package [26] [see Fig. 1(b)]. In contrast to the previous study of the $2b_2$ core-excited state [24] which was performed with CASSCF within an equivalent core approximation (H2F+), we have used the possibility with RASPT2 to explicitly calculate the core excitation with single occupation of the O1s orbital. Computational details can be found in our previous RIXS study of the vibrationally cold water molecule [7,9], which confirms the applicability of the model. The normal mode picture describes well the vibrational dynamics near the equilibrium. However, it fails for the higher excited vibrational states because of strong anharmonicity of the two-dimensional PESs. Due to this fact we choose to use valence coordinates [R_1, R_2, θ; see Fig. 1(a)] instead of normal mode coordinates for our numerical simulations. Using valence coordinates, we consider the Hamiltonian of the 2D stretching motion in the ith electronic state as

$$h_i = -\frac{1}{2\mu_1}\frac{\partial^2}{\partial R_1^2} - \frac{1}{2\mu_2}\frac{\partial^2}{\partial R_2^2} - \frac{\cos\theta_0}{m_O}\frac{\partial^2}{\partial R_1 \partial R_2} + V_i(R_1, R_2, \theta_0), \tag{2}$$

where θ_0 is the equilibrium bond angle, $\mu_\alpha = m_\alpha m_O/(m_\alpha + m_O)$ is the reduced mass with $\alpha = 1,2$, and $V_i(R_1, R_2, \theta)$ is the potential energy of the ith electronic state defined with

respect to its minimum. For the water molecule $\mu_1 = \mu_2 = \mu_H$, while for isotopic substitution of water HDO, studied here as well, $\mu_1 = \mu_H$ and $\mu_2 = \mu_D$. In order to compute the XAS and RIXS profiles we employ the time-dependent wave packet formalism [3] in the 2D representation [7,9] with the Hamiltonian (2), as is described in the following subsections.

B. X-ray absorption of vibrationally excited molecules

When the ground state is excited by an IR pulse, the x-ray absorption cross section reads

$$\sigma_{\rm abs}(\omega) = \int_0^\infty dt\ e^{(\imath(\Omega+\Delta)-\Gamma)t}\sigma(t), \quad \sigma(t) = \langle\psi_{\nu_0}|\psi_c(t)\rangle. \quad (3)$$

Here $\Omega = \omega - \omega_{\rm vert} + \epsilon_{\nu_0}$ is the detuning from the top of the absorption resonance, ϵ_{ν_0} is the vibrational energy of the initial vibrationally excited state $|\psi_{\nu_0}\rangle \equiv \psi_{s_0 a_0}$ of the ground electronic state, and $\Gamma = 0.08$ eV is the lifetime broadening of the core-excited state [7]. The vertical transition energy $\omega_{\rm vert}$ and the energy relative to the PES minima Δ are defined as

$$\omega_{\rm vert} = V_c(\mathbf{R}_0) - V_0(\mathbf{R}_0), \quad \Delta = V_c(\mathbf{R}_0) - V_c\big(\mathbf{R}_0^{(c)}\big), \quad (4)$$

where $\mathbf{R}_0(R_1^{(0)}, R_2^{(0)})$ and $\mathbf{R}_0^{(c)} = (R_1^{(c)}, R_2^{(c)})$ are the coordinates of the minima of the ground and core-excited states, respectively, and V_0 (V_c) is the potential energy of the ground (core-excited) state. The 2D core-excited wave packet in (3) can be computed as

$$|\psi_c(t)\rangle = e^{-\imath h_c t}|\psi_{\nu_0}\rangle, \quad (5)$$

with the Hamiltonian h_c defined according to (2), and with the initial condition $|\psi_c(0)\rangle \equiv \psi_{\nu_0}$ as the initial vibrational wave function of the ground state.

C. Resonant inelastic x-ray Raman scattering of vibrationally excited molecules

We consider a "quasi-elastic" scattering process, in which the system relaxes after the core excitation to the electronic ground but vibrationally excited state. In this case, we deal with vibrationally inelastic x-ray Raman scattering. We compute the cross section [3] of the RIXS process as a half-Fourier transform

$$\sigma(\omega,\omega') = P_f {\rm Re}\left[\int_0^\infty dt\ e^{\imath(\omega-\omega'+\epsilon_0)t} e^{-\Gamma_f t - \Gamma_w^2 t^2} c(t)\right] \quad (6)$$

of the autocorrelation function

$$c(t) = \langle\Phi_{\nu_0}(0)|\Phi_{\nu_0}(t)\rangle, \quad (7)$$

of the integrated core-excited $|\Phi_{\nu_0}(0)\rangle$ and final state $|\Phi_{\nu_0}(t)\rangle$ wave packets, defined as

$$|\Phi_{\nu_0}(t)\rangle = e^{-\imath h_f t}|\Phi_{\nu_0}(0)\rangle, \quad |\Phi_{\nu_0}(0)\rangle = \int_0^\infty dt_1 e^{-\Gamma t_1} e^{\imath(\Omega+\Delta)t_1}|\psi_c(t_1)\rangle. \quad (8)$$

The core-excited nuclear wave packet $|\psi_c(t)\rangle$ is computed using (5). In our case, the final electronic state is the ground state, so that $f = g$. The lifetime of the final state $\Gamma_f^{-1} \equiv \Gamma_0^{-1}$ is the vibrational lifetime which is incomparably larger (milliseconds) than the typical time of the wave packet dynamics (femtoseconds). Due to this, we use in the numerical simulations a Gaussian window function $\exp(-t^2\Gamma_w^2)$ (6) with $\Gamma_w = 12$ meV, which allows us to significantly decrease the computation time and which results in the width of the RIXS resonance, FWHM $= \Gamma_w 4\sqrt{2} = 40$ meV. We note that the window function, the only source of RIXS spectral broadening in our simulations, is smaller compared to the experimental instrumental broadening presently available (75 meV [7]). In Eq. (6), the P_f factor is defined by the experimental geometry and the symmetry of the final state. This factor changes only the absolute value of the cross section, not affecting vibrational effects discussed here; thus we use $P_f = 1$ in our calculations. As the transition origins from a higher ground vibrational states it is obvious that we will see anti-Stokes lines in the RIXS profile, corresponding to emission processes to the lower vibrational levels of the electronic ground state.

D. X-ray absorption in the Raman scattering mode

As already discussed in the Introduction, different methods are available for selective population of vibrational levels [13–16]. However, usually the pump IR field populates several vibrational levels $|\psi_{\nu_0}\rangle$ with the population weights ρ_{ν_0}. Then the probe x-ray field measures the cross section as a sum of particular absorption profiles from different initial vibrational states ν_0,

$$\sigma_{\rm abs}(\omega) = \sum_{\nu_0} \rho_{\nu_0}\sigma_{\nu_0}(\omega), \quad (9)$$

where the partial XAS cross section can be written using Fermi's golden rule in a time-independent representation

$$\sigma_{\nu_0}(\omega) \propto \sum_{\nu_c} \frac{\left|\langle\psi_{\nu_c}^c|\psi_{\nu_0}\rangle\right|^2}{\left(\Omega + \Delta - \epsilon_{\nu_c}\right)^2 + \Gamma^2}. \quad (10)$$

Here $|\psi_{\nu_c}^c\rangle$ is the 2D vibrational wave function of the core-excited electronic state, and ϵ_{ν_c} is the vibrational energy of the core-excited state $\nu_c = (s_c a_c)$.

The RIXS technique gives us a unique opportunity to measure the XAS absorption $\sigma_{\nu_0}(\omega)$ from certain initial vibrational states ψ_{ν_0}. The idea to measure XAS in the resonant x-ray scattering mode has been implemented successfully to record the XAS profile of CO with extremely high resolution [27] using resonant Auger measurements. In the present paper, we propose to apply this technique for the RIXS scheme. For this purpose, we need first to measure the RIXS cross section [27] (see also Sec. III C)

$$\left|\sum_{\nu_c} \frac{\langle\psi_{\nu_f}|\psi_{\nu_c}^c\rangle\langle\psi_{\nu_c}^c|\psi_{\nu_0}\rangle}{\Omega + \Delta - \epsilon_{\nu_c} + \imath\Gamma}\right|^2 \quad (11)$$

on the "Raman ridge"

$$\omega' = \omega + \epsilon_{\nu_0} - \epsilon_{\nu_f}, \quad (12)$$

describing the energy conservation law for the RIXS process [3]. Here ψ_{ν_f} is the final vibrational state of the RIXS transition.

One can expect that the absorption cross section in the scattering mode will approximately coincide with the conventional XAS profile for the unshifted line: $\omega' = \omega$, $\epsilon_{\nu_f} = \epsilon_{\nu_0}$. In order to obtain a partial XAS cross section, $\sigma_{\nu_0}(\omega)$, in the Raman

mode (XASRM) we need to measure the RIXS cross section $\sigma(\omega',\omega)$ as a function of excitation energy ω along the Raman ridge for the unshifted line $\epsilon_{\nu_f} = \epsilon_{\nu_0}$. In this case, the RIXS cross section (11)

$$\sigma(\omega,\omega'=\omega,\nu_f=\nu_0) \propto \left| \sum_{\nu_c} \frac{\left|\left\langle \psi^c_{\nu_c} \middle| \psi_{\nu_0} \right\rangle\right|^2}{\Omega + \Delta - \epsilon_{\nu_c} + \imath\Gamma} \right|^2 \quad (13)$$

is very similar to the XAS cross section (10), except for two differences. The first distinction is that the XASRM cross section (13) contains a lifetime vibrational interference (LVI) contribution [28], which is not present in the conventional XAS cross section $\sigma_\nu(\omega)$ (10). As we will show in Sec. III C the effect of the LVI is rather weak in the studied system. The second difference between the XASRM (13) and XAS (10) cross sections is that the XASRM cross section is proportional to the second power of the Franck-Condon factors, which results in a sharpening of the XASRM vibrational resonances. To achieve a better correspondence between the XASRM and XAS profiles it is sufficient to take the square root from the cross section (13) (see Sec. III C):

$$\sigma_{\mathrm{XASRM}}(\omega) = \sqrt{\sigma(\omega,\omega'=\omega,\nu_f=\nu_0)}. \quad (14)$$

III. RESULTS AND DISCUSSION

In what follows, we consider the six initial vibrational states $\psi_{s_0a_0}$ of the electronic ground state $(s_0a_0) = (00),(10),(01),(20),(11),(02)$ (shown in order of increasing energy). The incident photon energy ω is tuned near the resonances with the two lowest $4a_1$ and $2b_2$ core-excited states of the water molecule having dissociative and bound character, respectively. We use a two-step theoretical approach. First, we compute the 2D PESs of the ground and core-excited states [Fig. 1(b)] using the RASSCF method followed by the second-order perturbation theory method RASPT2 implemented in the MOLCAS package [26]. The computed core-excited PESs were slightly shifted ($\lesssim -0.1$ eV) in order to fit the experimental core-excitation energy positions measured for the case of the ground vibrational level ψ_{00} [22,24]. The *ab initio* PESs are furthermore used for the time-dependent solution of the 2D Schrödinger equation and spectral simulations, as explained in Sec. II, employing the locally developed eSPec program [10,12].

A. X-ray absorption

The pump-probe scheme for XAS is depicted in Fig. 2. The theoretical XAS profiles around the dissociative $4a_1$ and the bound $2b_2$ states are shown in Figs. 3 and 4, respectively, for six initial vibrational excited states of the molecule $\psi_{00},\ldots,\psi_{02}$. In the case of the dissociative $4a_1$ state we compare the XAS formation for the symmetric H_2O and nonsymmetric HDO molecules. The sensitivity of the spectral band to the initial vibrational state comes from two qualitatively different effects. First, the envelope of the XAS band reflects the coordinate distribution of the square of the initial vibrational wave function (IVWF) according to the reflection principle. Second, the XAS vibrational fine structure is sensitive to the symmetry of the IVWF due to the selection rules.

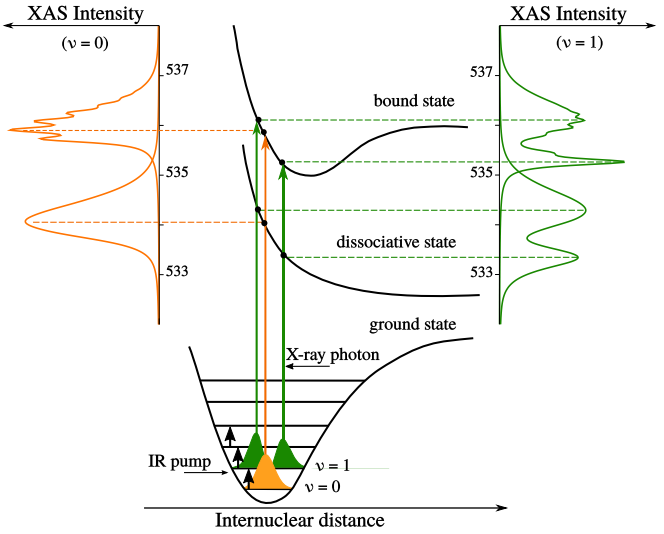

FIG. 2. Formation of the x-ray absorption profile from different initial vibrational states according to the reflection principle. The left-hand side shows XAS from the lowest vibrational level, while XAS in the right-hand side corresponds to the core excitation from the first excited vibrational state having one node.

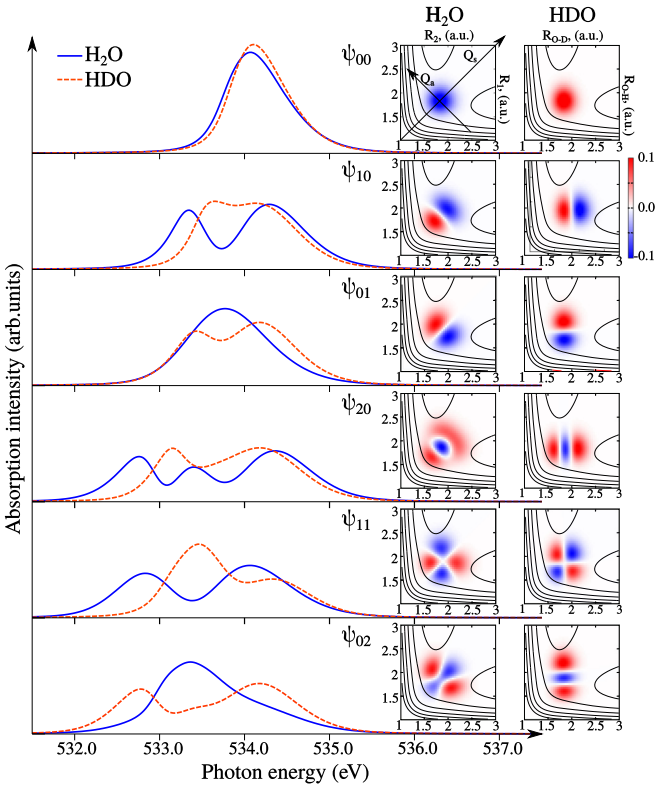

FIG. 3. XAS of H_2O (solid lines) and HDO (dashed lines) molecules at the dissociative $4a_1$ resonance from the six lowest vibrational levels. The right-hand side panels present the initial vibrational wave functions of the molecules together with the $4a_1$ core-excited state PES drawn by the isolines. The initial vibrational states of HDO ψ_{n_D,n_H} are assigned using vibrational quantum numbers n_D and n_H of the vibrations localized on the OD and OH bonds, respectively.

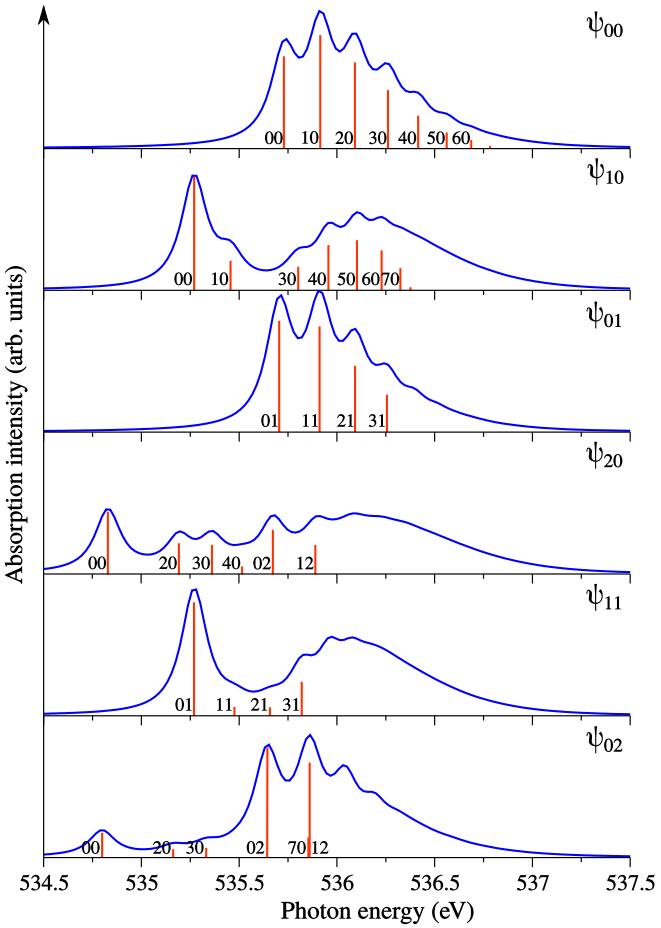

FIG. 4. XAS of the bound $2b_2$ core-excited state of H_2O molecule for six lowest initial vibration states $\psi_{00} \ldots \psi_{02}$ shown in Fig. 3. Vertical lines display calculated Franck-Condon factors.

1. *Reflection principle and vibrational wave function mapping*

One-dimensional (1D) reflectional principle. The overall shape (envelope) of the absorption profiles in Figs. 3 and 4 can easily be explained using the so-called reflection principle, well known in the photoelectron spectroscopy [19,29], resonant Auger scattering [30,31], and RIXS spectroscopy [32] communities. In a very similar way it can be applied here to XAS. In the 1D case the reflection principle has a simple graphical interpretation; as is illustrated in Fig. 2, the vertical transitions to the classical turning points produce absorption intensity which is proportional to the square of the ground state vibrational wave function. This gives the opportunity to map the square of the initial vibrational wave function [19,29–32]. Indeed, the lowest vibrational wave function with a single maximum produces a single peak XAS, while the squared vibrational wave function having two maxima results in a bimodal XAS spectrum. The reflection principle in XAS is quite accurate for a dissociative core-excited state. One should notice, however, that the XAS profile reproduces only approximately the square of the IVWF, because simple mirror reflection is valid only for a linear potential $dV_c/dR =$ const. The reflection technique can be applied to the bound core-excited states as well. For a clear reflection in this case, the potential energy curve minimum must be shifted considerably relative to the ground state minimum. Contrary to the dissociative core-excited state, the XAS profile of the bound core-excited state consists of set of narrow vibrational resonances with intensity distribution given by the Franck-Condon factors. The reflectional principle describes only the envelope of the XAS vibrational progression (Fig. 2), which approximately repeats the coordinate distribution of the square of the IVWF (ψ_{ν_0}). This explains why the envelope of the XAS is very sensitive to the spatial shape of ψ_{ν_0}. For example, the number of peaks in the XAS envelope is equal to $m + 1$, where m is the number of nodes of ψ_{ν_0}.

2D reflectional principle. The 1D reflection principle helps to understand the XAS formation in the 2D case applying the 1D principle along the symmetric $Q_s \sim R_1 + R_2$ and antisymmetric $Q_a \sim R_1 - R_2$ coordinates. As one can see from Fig. 1, the PESs (the same for the H_2O and HDO molecules) of the ground and core-excited states are symmetric along the antisymmetric stretching coordinate Q_a, which is important for the XAS formation, as demonstrated below. Let us consider in Fig. 3 the core excitation to the dissociative $4a_1$ state from different IVWFs of the H_2O molecule. Apparently, in the case of ψ_{00} IVWF the XAS has a single peak due to single maximum of the ψ_{00} shape in both the Q_s and Q_a directions (Fig. 3). It is also easy to associate the double maximum structure of the $|\psi_{10}|^2$ IVWF along Q_s with the double-peak XAS spectrum by applying the 1D reflectional principle along Q_s coordinate (Fig. 3). The 1D reflectional principle along Q_a does not bring an additional maxima in this case, because $|\psi_{10}|^2$ has only one maximum along this coordinate. The picture changes qualitatively for the excitation from the ψ_{01} IVWF. Contrary to the ψ_{10} IVWF, the XAS profile has a single peak in spite of the two maxima of the $|\psi_{01}|^2$ shape (Fig. 3). The reason for this unexpected effect is the symmetry of the core-excited PES along Q_a, where two maxima of $|\psi_{01}|^2$ are presented. Due to this circumstance the transition energies near the two maxima of IVWF ψ_{01} are exactly the same and the XAS has only one degenerate peak. Similarly, the formation of the XAS profile for higher IVWF ψ_{20}, ψ_{11}, and ψ_{02}, shown in Fig. 3, can be explained.

Moving to a partially deuterated water molecule, it is interesting to note that the replacement of a hydrogen by a deuterium changes qualitatively the XAS profile, as one can see from a comparison of the H_2O and HDO spectra (Fig. 3). The main reason for this is the symmetry breaking followed by the localization of the stretching vibrations on the OD or OH bonds of the ground state HDO molecule (for more details see Ref. [33]). Due to the localization we assign the IVWF of HDO as ψ_{n_D,n_H}, where n_D and n_H are the vibrational quantum numbers of the OD and OH vibrations, respectively. It is important to note that the bond breaking in the dissociative $4a_1$ core-excited state of HDO is also localized [33]. The double-peak XAS spectra for ψ_{10} and ψ_{01} IVWFs can be easily understood by applying the 2D reflection principle to the double-peak shape of the IVWFs aligned along the OD and OH bonds. Contrary to the reflection principle along Q_a for H_2O, there is no symmetry of the core-excited PES along the OD and OH coordinates and the transition energy degeneracy observed in ψ_{01} XAS of H_2O is lifted. This results in a double-peak XAS for the ψ_{01} excitation in HDO. The difference in the ψ_{10} and ψ_{01} XAS spectra of HDO is due to the slower dissociation of

heavier deuterium atom in comparison to the light hydrogen in the dissociative $4a_1$ core-excited state [33].

Contrary to the smooth XAS profile in the case of the dissociative $4a_1$ state, the XAS profile of the bound $2b_2$ core-excited state clearly shows vibrational structure (4). The envelope of the XAS spectrum here shows the same tendency as was explained for the dissociative $4a_1$ state according to the reflection principle. For the core excitation from the lowest initial ψ_{00} state we can discern only a rather small range of the vibration transitions limited by the Frank-Condon region. In order to excite more vibrational levels of the core-excited state, higher IVWFs should be used. This results in a broader XAS profile with more vibrational resonances (Fig. 4), which is important for a mapping of the core-excited potential in a wider energy range [34].

2. *Selection rules in XAS*

First, let us consider the XAS for the bound core-excited state $2b_2$ of the H_2O molecule. The amplitude of the XAS transition $\psi_{s_0a_0} \rightarrow \psi^c_{s_ca_c}$ is defined by the FC overlap $\langle \psi^c_{s_ca_c} | \psi_{s_0a_0} \rangle$. Both ground and core-excited PESs (Fig. 1) are symmetric with respect to the reflection $Q_a \rightarrow -Q_a$ relative to the Q_s axis, which results in the following symmetry property of the vibrational wave functions of these bound states

$$\psi_{sa}(Q_s, -Q_a) = (-1)^a \psi_{sa}(Q_s, Q_a) \tag{15}$$

and of the FC amplitude

$$\langle \psi^c_{s_ca_c} | \psi_{s_0a_0} \rangle = (-1)^{a_c+a_0} \langle \psi^c_{s_ca_c} | \psi_{s_0a_0} \rangle. \tag{16}$$

This identity gives the following selection rule: Only XAS transitions with

$$a_c + a_0 = \text{even} \tag{17}$$

are allowed. This selection rule is valid only for the bound-bound XAS transitions. The selection rules are absent for the dissociative $4a_1$ core-excited state due to degeneracy of symmetric and antisymmetric motions in the dissociative continuum. The symmetry selection rule for antisymmetric vibrations is seen clearly in the XAS spectral profile of the bound $2b_2$ core-excited state (Fig. 4). Indeed, the XAS vibrational progression consists of only even antisymmetric vibrational states $a_c = 0,2,\ldots$ when the antisymmetric quantum number of initial vibrational state is even: $\psi_{00}, \psi_{10}, \psi_{20}, \psi_{02}$. The IR excitation of odd antisymmetric vibrational states (ψ_{01}, ψ_{11}) results in an XAS vibrational progression with odd antisymmetric states $(s_ca_c) = (01),(11),(21),(31),\ldots$. Thus selection rule (17) allows one to separate the symmetric and antisymmetric vibrational progressions of the bound core-excited state by varying the symmetry of the IVWF. This provides an opportunity to map selectively the PESs of core-excited states along symmetric and antisymmetric coordinates.

B. RIXS from vibrationally excited molecules

RIXS is a well-established technique for probing of the electronic ground and valence excited states of neutral molecules. Here we consider a particular case of RIXS, electronically elastic x-ray scattering back to the ground state, the so-called "quasi-elastic" scattering channel. Due to the nuclear dynamics in the core-excited state, a vibrational progression is usually observed in RIXS to the ground state, which allows one to study the ground state potential along particular modes [6,7]. In the present section we will discuss RIXS from vibrationally excited molecules. The RIXS spectra are computed here for the excitation energy ω tuned into the resonance with the lowest vibration level $\nu_c = (00)$ of the bound $2b_2$ core-excited state, and in resonance with the vertical transition energy in the case of the dissociative $4a_1$ core-excited state, $\omega = \omega_{\text{vert}} - \epsilon_{\nu_0}$.

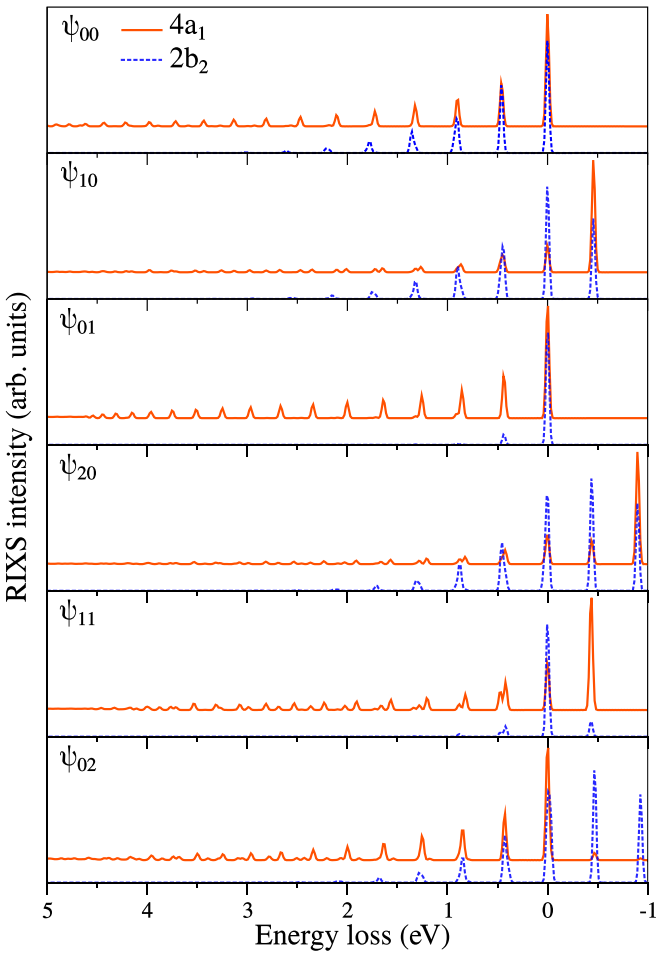

FIG. 5. RIXS spectra of a vibrationally excited H_2O. The plots are marked with the initial vibrational wave functions used in the RIXS simulations. The $4a_1$ RIXS spectra are shifted vertically for better visibility.

In RIXS, similar to the x-ray absorption, the reflection principle can be employed for analysis of the spectra [31,32,35]. It was shown [32,35] that the envelope of the RIXS profile approximately copies the shape of square of the wave packet in the core-excited state $|\Phi_{\nu_0}(0)\rangle$. For example, the core-excited wave packet in the dissociative state propagates quickly towards the long bond-length range, which results in a wide vibrational progression in the $4a_1$ RIXS band up to $\omega - \omega' = 6$ eV energy loss (Fig. 5). In contrast, the core-excited wave packet on the $2b_2$ state is confined to rather short bond lengths, and thus only a relatively short vibrational progression is observed in this case (Fig. 5). Since the wave packet in the

core-excited state is sensitive to the spatial distribution of the IVWF (see Sec. III A 1), the envelope of the RIXS profile depends on the IVWF as well (Fig. 5).

A conventional RIXS spectrum from the lowest vibrational level $\nu_0 = 00$ consists of the Stokes resonances $\omega - \omega' = \epsilon_{\nu_f} - \epsilon_{00} > 0$ and unshifted or elastic line $\omega - \omega' = 0$. In contrast, the studied here RIXS from excited vibrational level ν_0 also possess anti-Stokes lines with negative energy loss $\omega - \omega' = \epsilon_{\nu_f} - \epsilon_{\nu_0} < 0$. From Fig. 5 one can see that RIXS starting from an even antisymmetric initial state of the $n = s_0 + a_0$ group results in n anti-Stokes lines. The lowest anti-Stokes resonance corresponds to the RIXS transition to the zero-point energy level ψ_{00} of the ground electronic state. Let us now show how the IR excitation of the vibrational state of certain symmetry can be used for experimental assignment of the close-lying vibrational levels in the ground state.

1. Selection rules in RIXS

A selection rule for the RIXS process follows directly from the amplitude of the RIXS transition $\psi_{\nu_0} \to \psi_{\nu_f}$ to the final vibrational state [7,33]

$$\langle \psi_{\nu_f} | \Phi_{\nu_0}(0) \rangle, \tag{18}$$

where $|\Psi_{\nu_0}(0)\rangle$ contains the IVWF ψ_{ν_0} as follows from Eqs. (5) and (8). The evolution operator $\exp(-\imath h_c t)$ is symmetric with respect to inversion $Q_a \to -Q_a$, implying that the symmetry of the wave packet $|\Phi_{\nu_0}(0)\rangle$ is the same as the symmetry of the initial vibrational state $\psi_{s_0 a_0}(Q_s, -Q_a) = (-1)^{a_0} \psi_{s_0 a_0}(Q_s, Q_a)$ (15). This results in the following selection rule for allowed RIXS transitions

$$a_0 + a_f = \text{even}, \tag{19}$$

where a_0 and a_f are the vibrational quantum numbers of the antisymmetric mode in the ground and final electronic states, respectively. Contrary to the XAS transitions, the selection rule (19) remains valid irrespective of whether the core-excited state is bound or dissociative. According to this selection rule RIXS from an even (odd) antisymmetric stretching state $a_0 = 2k$ ($a_0 = 2k + 1$) ends up only in even (odd) final states (see Fig. 6). To show the effect of the selection rule (19) let us compare details of RIXS spectra from IVWF of opposite parities ψ_{10} and ψ_{01} (Fig. 7). The initial state ψ_{10} leads to RIXS transitions to even antisymmetric states $a_f = 0,2,4,\ldots$, while only the odd final states $a_f = 1,3,\ldots$ are populated when the initial state is ψ_{01} for both dissociative $4a_1$ and bound $2b_2$ core-excited states. Thus the pump-probe technique offers a unique opportunity to measure separately even $\psi_{s_f,2k}$ and odd $\psi_{s_f,2k+1}$ vibrational progressions.

2. Propensity rules in RIXS

Besides the strict selection rule (19), the RIXS spectra (Fig. 7) exhibit also suppression of particular symmetry allowed vibrational states. These propensity rules (Fig. 6) origins from a small Franck-Condon overlap (18) of the wave packet $|\Phi_{\nu_0}(0)\rangle$ and final vibrational state ψ_{ν_f}. Indeed, starting from the group $n = s_0 + a_0 = 3$ the RIXS peaks $\psi_{n,0}$ are strongly suppressed for the ψ_{10} IVWF in the $2b_2$ RIXS spectrum [Fig. 7(a)]. RIXS through the dissociative $4a_1$ state shows the opposite trend: the resonance $\psi_{n-2,2}$ has smaller

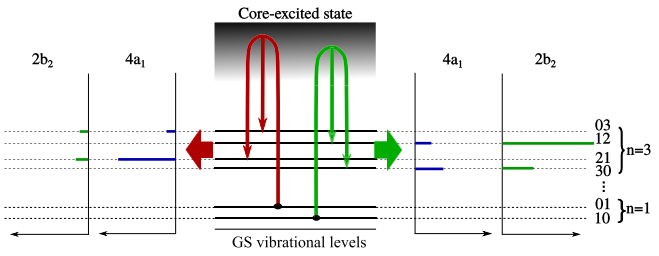

FIG. 6. Selection and propensity rules for RIXS. The vertical red (left) and green (right) arrows show the symmetry allowed RIXS channels, which starts from the initial vibrational states ψ_{01} and ψ_{10}, respectively. Horizontal lines show the intensities of the RIXS transitions, which are allowed according to the selection rules (19). The resonances (03) for the $4a_1$ RIXS and (30) for the $2b_2$ RIXS are suppressed due to the propensity rules (see text). The energies of the vibrational levels of the ground state of H_2O with respect to the zero-point level ϵ_{00}: ϵ_{10}–$\epsilon_{00} = 0.4588$ eV, ϵ_{01}–$\epsilon_{00} = 0.4680$ eV, ϵ_{30}–$\epsilon_{00} = 1.3222$ eV, ϵ_{21}–$\epsilon_{00} = 1.3229$ eV, ϵ_{12}–$\epsilon_{00} = 1.3581$ eV, ϵ_{03}–$\epsilon_{00} = 1.3763$ eV.

intensity than the $\psi_{n,0}$ peak. The propensity rules for the ψ_{01} IVWF are different [Fig. 7(b)]. Now the $\psi_{n,0}$ resonances are suppressed in the the $2b_2$ RIXS starting from $n = 4$ in contrast to the $4a_1$ RIXS, where the $\psi_{n-3,3}$ resonances are suppressed for $n \geqslant 3$. To understand the propensity rules, which originates from the RIXS amplitude (18), let us analyze the spatial distribution of the core-excited wave packet $|\Phi_{\nu_0}(0)\rangle$ in relation to the final vibrational wave functions ψ_{ν_f} (see Fig. 8).

In the case of the $2b_2$ core-excited state, the wave packet $|\Phi_{10}(0)\rangle$ (IVWF is ψ_{10}) is localized along the Q_s coordinate

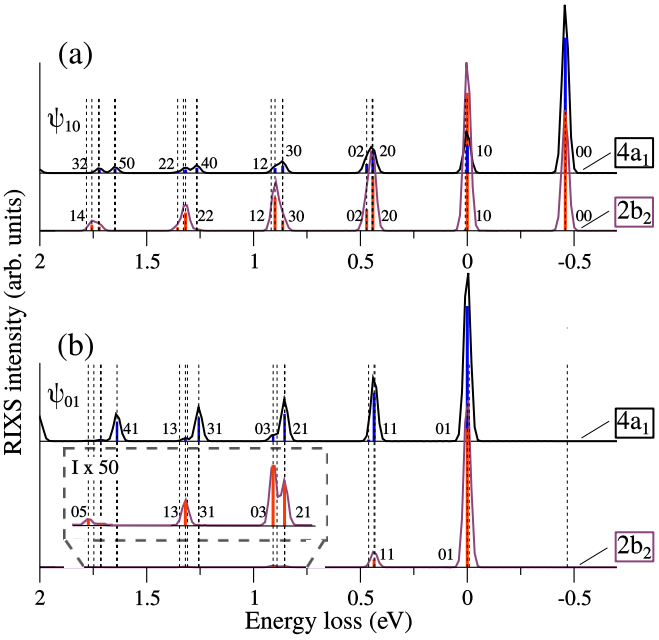

FIG. 7. Fine structure of the RIXS spectrum of H_2O molecule with initial vibrational state ψ_{10} (a) and ψ_{01} (b). The vertical dashed lines show the ground state eigenvalues. The vertical solid lines show the Frank-Condon factors for the emission from the $4a_1$ and $2b_2$ states. The allowed vibrational states are assigned.

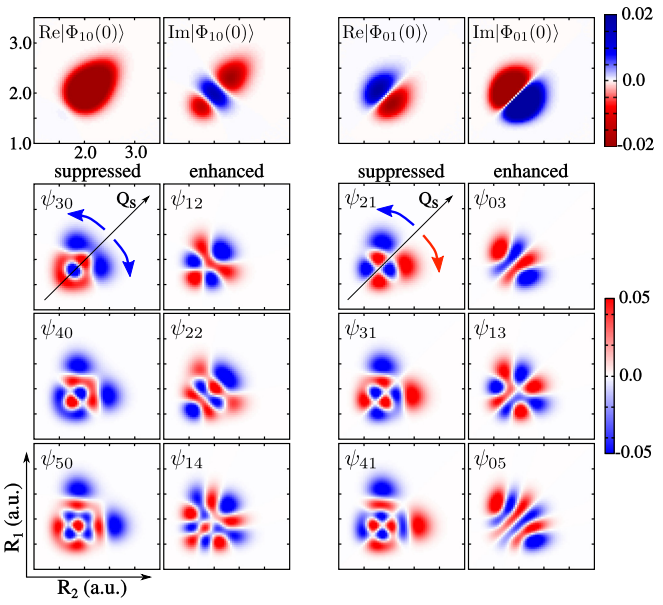

FIG. 8. Physical picture of the propensity rules for RIXS via the $2b_2$ core-excited state. The propensity rule originates from the RIXS amplitude (18) given by the overlap of the wave packet $\Phi_{10}(0)$ or $\Phi_{01}(0)$ (upper panels) with the final vibrational states ψ_{sa} (lower panels). See text for details.

(18), as it is defined by the shape of the $2b_2$ PES (Fig. 7). The main contribution to the Franck-Condon factors for transitions to the ψ_{30}, ψ_{40}, and ψ_{50} vibrational states is given by the overlap with two lobs at $R_{1,2} \approx 2.5$ a.u. [7]. These lobes moves apart with increasing n, thereby quenching the overlap (18) and thus suppressing the intensity of the lines ψ_{n0} for higher n in the RIXS spectra (Fig. 7). In contrast, the final vibrational wave functions ψ_{12}, ψ_{22}, and ψ_{14} show a large amplitude along the diagonal Q_s resulting in favorable overlap with $|\Phi_{10}(0)\rangle$ and, hence, strong RIXS intensities. The explanation of the propensity rules for the initial state ψ_{01} is similar (see the right-hand-side panel in Fig. 8). However, now we have to consider the RIXS transitions to the odd antisymmetric final states allowed by the RIXS selection rule (19).

When the scattering is going through the dissociative $4a_1$ state the picture is inverted in perfect agreement with the RIXS spectra (Fig. 7). The reason for this is that the wave packet $|\Phi_{10}(0)\rangle$ is now localized along the bonds, more precisely, along the valleys of the $4a_1$ dissociative potential (Fig. 1). Let us stress here that RIXS through the two core-excited states with different PES shape and thus different localization of the nuclear wave packet (along and between the bonds for the $4a_1$ and $2b_2$ states, respectively) allows one to resolve close-lying vibrational states due to the different propensity rules even for moderate spectral resolution (40 meV) used in the simulations [see, for example, (12) and (30) resonances in Fig. 7(a) and (13) and (31) resonances in Fig. 7(b)]. This effect was nicely demonstrated in a recent RIXS experiment for the ψ_{00} initial state of H_2O [7].

It is instructive to consider RIXS 2D maps in the $(\Omega, \omega - \omega')$ plane (Fig. 9). The RIXS spectra display here a strong sensitivity to the initial vibrational state $\nu_0 = (00),(10),(01)$ which originates from the selection and propensity rules, as well as the Franck-Condon factors. This allows one to probe vibrational levels of both ground and core excited states. Furthermore, the improvement of spectral resolution makes it possible to resolve close-lying vibrational levels of each nth group (see Sec. III C) and to map the ground state PES along different modes [36].

C. XAS measured in the Raman mode

Finally, we want to bring attention to the value of measuring partial XAS in the x-ray Raman mode and its information content. In order to investigate XASRM (11), 14), let us first consider 2D RIXS maps for the $2b_2$ resonance for the two IVWFs ψ_{00} and ψ_{10} (Fig. 10). Each diagonal ridge in the case of perfect resolution corresponds to a particular final vibrational state $\nu_f = (00),(10),(01),\ldots$ and initial state $\nu_0 = (00),(10)$ according to the Raman dispersion law (12). The lowest ridge in RIXS from the initial vibrational state $\nu_0 = (00)$ [Fig. 10(a)] is related to the elastic RIXS resonance ($\omega' = \omega$). When RIXS starts from excited vibrational state $\nu_0 = (10)$ [Fig. 10(b)] the lowest ridge ($\nu_f = (00)$) corresponds to the anti-Stokes line, while the elastic RIXS ($\omega' = \omega$) is described by the second ridge ($\nu_f = \nu_0 = (10)$). The maxima along each ridge correspond to the vibrational resonances of the

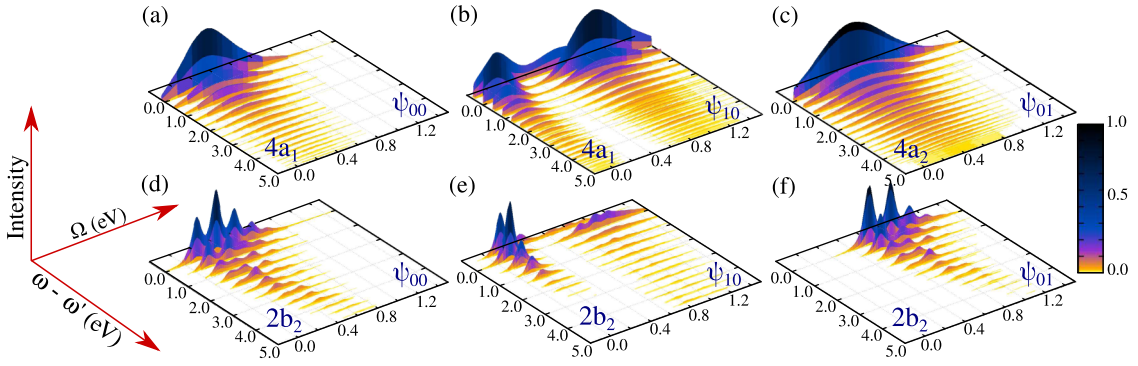

FIG. 9. RIXS maps in the $(\Omega, \omega - \omega')$ plane for the tree lowest initial states ψ_{00}, ψ_{10}, and ψ_{01}. The panels (a–c) and (c–d) correspond to the scattering via the $4a_1$ and $2b_2$ core-excited states of H_2O, respectively.

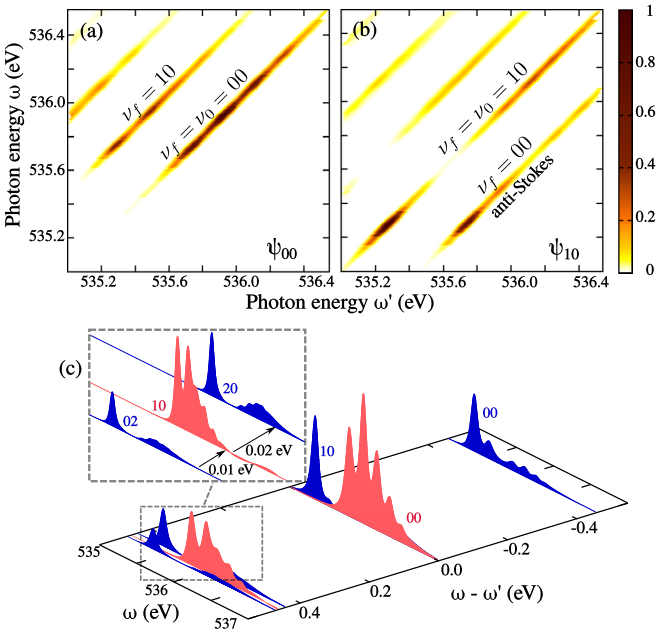

FIG. 10. 2D maps of RIXS from the initial (a) ψ_{00} and (b) ψ_{10} vibrational states. The scattering occurs via the $2b_2$ core-excited state of H_2O. Each RIXS map is normalized to its maximal value. Panel (c) shows the partial RIXS spectra for perfect spectral resolution for equal populations of the ψ_{00} and (b) ψ_{10} levels. The red (gray) and blue (black) RIXS profiles in the panel (c) correspond to the initial vibrational states ψ_{00} and ψ_{10}, respectively.

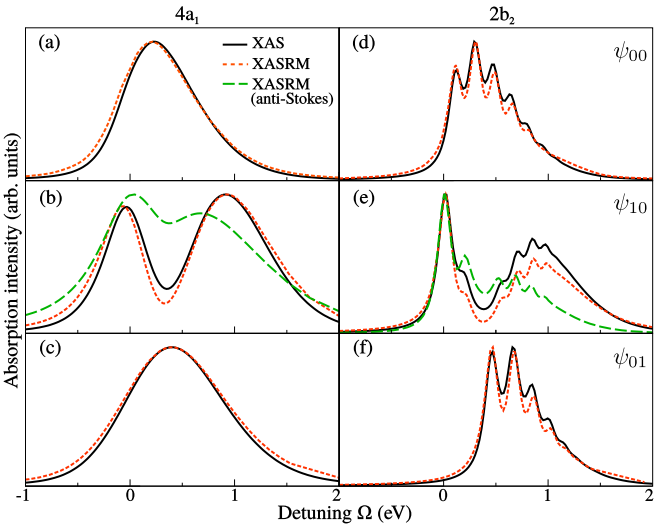

FIG. 11. XASRM spectra (14) (short dashed lines) along the elastic ridges ($\omega = \omega'$) for $4a_1$ (a–c) and $2b_2$ (d–f) core-excited states. The solid lines show conventional XAS profiles (10). The RIXS from the IVWF ψ_{00}, ψ_{10}, and ψ_{01} are shown in panels (a, d), (b, e), and (c, f), respectively. The large dashed line represents the XASRM profile based on the anti-Stokes line $\psi_{10} \to \psi_{00}$ ($\omega - \omega' = -0.46$ eV) [see Eq. (20)]. All spectra are normalized to their maximum values.

core-excited state according to the cross section in Eq. (11). In the case of selective population the initial states $\nu_0 = (00)$ and $\nu_0 = (10)$ the best way to measure a partial XASRM from an individual initial state is to take the square root from the recorded RIXS profile along the unshifted ridge ($\nu_f = \nu_0$). The corresponding calculations based on Eqs. (13) and (14) display rather good agreement with the true XAS absorption profile (10) as is shown in Fig. 11 for both bound $2b_2$ and dissociative $4a_1$ core-excited states.

However, the selective population of different initial vibrational states is a rather difficult task. When several vibrational levels are initially populated, the XASRM profile (13)–(14) includes contributions from all IVWFs. For example, when both the ψ_{00} and ψ_{10} states are initially populated, the XASRM will be the sum of the unshifted ridges ($\nu_f = \nu_0, \omega' = \omega$) from the 2D RIXS maps in Fig. 10(a) and Fig. 10(b). This is exactly the same problem we face in conventional XAS measurements [see Eq. (10)].

The presence of the anti-Stokes line in RIXS of vibrationally excited molecules provides an unique opportunity to measure the partial XAS profile from a particular initial vibrational state ν_0. Indeed, the anti-Stokes ridge is present only in the RIXS of a vibrationally excited molecule [Fig. 10(b)], and it is absent in an unexcited molecule [Fig. 10(a)]. The RIXS spectrum for $\nu_0 = 10$ along the anti-Stokes ridge $\nu_f = (00)$ is given by

$$\sigma(\omega,\omega' = \omega + \epsilon_{10} - \epsilon_{00}) \propto \left| \sum_{\nu_c} \frac{\langle \psi_{00} | \psi^c_{\nu_c} \rangle \langle \psi^c_{\nu_c} | \psi_{10} \rangle}{\Omega + \Delta - \epsilon_{\nu_c} + \imath\Gamma} \right|^2 . \tag{20}$$

One should mention that the IR light also can populate the $\nu_0 = (01)$ level. However, the anti-Stokes line is the symmetry forbidden in this case. Similar to Eq. (14) we compute the XASRM spectrum taking the square root from the cross section (20) (see Fig. 11, dashed line). In spite of some disagreement with the XAS profile, the XASRM spectra based on the anti-Stokes line show all the main features of the absorption spectra, as well as accurate positions of the vibrational resonances in the $2b_2$ core-excited state. Similarly, the anti-Stokes lines for initial vibrational levels from higher groups $n > 1$ can be used to single out the partial XAS contribution from these states.

The improving of the spectral resolution brings another possibility to separate contributions from different IVWFs. As is shown in Fig. 10(c) the ridges from the IVWF ψ_{00} (red or gray profile) and ψ_{10} (blue or black profile) near $\omega - \omega' \approx 0.38$ eV can be resolved only when the spectral resolution is better than 1 meV. Such quasi-degeneracy is a general phenomenon for higher vibrational levels from the same group n. However, with the improvement of the spectral resolution of RIXS (see Sec. I) one can resolve close-lying ridges in RIXS from a given initial vibrational state and thus distinguish contributions from the different initial states ψ_{ν_0} [Fig. 10(c)]. The only exception is the elastic scattering line $\nu_f = \nu_0$, where one cannot separate contributions of different initial vibrational states because the corresponding RIXS spectra are lying on the same ridge $\omega - \omega' = 0$ [Fig. 10(c)].

IV. CONCLUSIONS

We have presented a theoretical study of XAS and RIXS spectroscopy applied to vibrationally excited molecules, using water molecule as a showcase. We have demonstrated the advantage of using IR-pump–x-ray-probe methodology for

studies of symmetric molecules, where the symmetry of a selected initial vibrational state makes it possible to address a particular vibrational mode in the core-excited state and therefore also in the final vibrational state of the RIXS process. The excited vibrational wave function of the ground electronic state is more broadly distributed over nuclear coordinates in comparison to the lowest vibrational wave function. This, according to the reflection principle, allows one to study an extended energy range of the potential energy surfaces of the core-excited and final states. The pump-probe XAS spectra reflect the shape of the vibrational wave function of the H_2O molecule along symmetric and antisymmetric coordinates contrary to HDO, for which the spectra are defined by coordinate distribution of the wave functions along the bonds. It is shown that the reflection principle is qualitatively different for symmetric and antisymmetric initial vibrational states of H_2O due to different nonlinearity of the PES of the core excited state along these modes. It is demonstrated that XAS measured in the x-ray Raman mode makes it possible to obtain partial spectra initiated from different vibrational levels of the ground state. The symmetry selection and propensity rules inherent in the pump-probe technique, together with the selective excitation to core-excited states with different spatial shape of the potential energy surfaces, makes it possible to probe the ground state modes along selected directions, which can be used for mapping of the PESs.

Our study indicates that the proposed technique can be applied to advanced symmetry-resolved studies of polyatomic molecules and ground state vibrational excitation followed by x-ray absorption and that it can also be used for controlling chemical reactions as well as ultra-fast fragmentation and isomerization processes in short-lived core-excited states.

ACKNOWLEDGMENTS

This work was supported by the Russian Science Foundation (Grant No. 16-12-10109), the Knut and Alice Wallenberg Foundation (Grant No. KAW-2013.0020), the Swedish Research Council (VR), and Carl Tryggers Stiftelse för Vetenskaplig Forskning. M.O. acknowledges funding from the Helmholtz Virtual Institute VI419 "Dynamic Pathways in Multidimensional Landscapes." R.C.C. and V.V.C. acknowledge the Conselho Nacional de Desenvolvimento Científico e Tecnológico (CNPq–Brazil). Numerical simulations were performed using Swedish National Infrastructure for Computing (SNIC).

[1] P. Maksyutenko, M. Grechko, T. R. Rizzo, and O. V. Boyarkin, Phil. Trans. R. Soc. A **370**, 2710 (2012).
[2] M. Grechko, O. V. Boyarkin, T. R. Rizzo, P. Maksyutenko, N. F. Zobov, S. V. Shirin, L. Lodi, J. Tennyson, A. G. Császár, and O. L. Polyansky, J. Chem. Phys. **131**, 221105 (2009).
[3] F. Gel'mukhanov and H. Ågren, Phys. Rep. **312**, 87 (1999).
[4] L. J. P. Ament, M. van Veenendaal, T. P. Devereaux, J. P. Hill, and J. van den Brink, Rev. Mod. Phys. **83**, 705 (2011).
[5] A. Pietzsch, F. Hennies, P. S. Miedema, B. Kennedy, J. Schlappa, T. Schmitt, V. N. Strocov, and A. Föhlisch, Phys. Rev. Lett. **114**, 088302 (2015).
[6] S. Schreck, A. Pietzsch, B. Kennedy, C. Såthe, P. S. Miedema, S. Techert, V. N. Strocov, T. Schmitt, F. Hennies, J.-E. Rubensson, and A. Föhlisch, Sci. Rep. **7**, 20054 (2016).
[7] R. C. Couto *et al.*, Nat. Commun. **8**, 14165 (2017).
[8] M. Le Tacon, A. Bosak, S. M. Souliou, G. Dellea, T. Loew, R. Heid, K. Bohnen, G. Ghiringhelli, M. Krisch, and B. Keimer, Nat. Phys. **10**, 52 (2014).
[9] R. C. Couto, Coupled electron-nuclear dynamics in inelastic X-ray scattering, Ph.D. thesis, KTH, Sweden, 2016.
[10] F. F. Guimarães, V. Kimberg, V. C. Felicíssimo, F. Gel'mukhanov, A. Cesar, and H. Ågren, Phys. Rev. A **72**, 012714 (2005).
[11] F. F. Guimarães, V. Kimberg, V. C. Felicíssimo, F. Gel'mukhanov, A. Cesar, and H. Ågren, Phys. Rev. A **71**, 043407 (2005).
[12] V. C. Felicíssimo, F. F. Guimarães, F. Gel'mukhanov, A. Cesar, and H. Ågren, J. Chem. Phys. **122**, 094319 (2005).
[13] U. Gaubatz, P. Rudecki, S. Schiemann, and K. Bergmann, J. Chem. Phys. **92**, 5363 (1990).
[14] C. Leonard, G. Chambaud, P. Rosmus, S. Carter, and N. C. Handy, Phys. Chem. Chem. Phys. **3**, 508 (2001).
[15] M. Becker, U. Gaubatz, K. Bergmann, and P. L. Jones, J. Chem. Phys. **87**, 5064 (1987).
[16] G. K. Paramonov and O. Kühn, J. Phys. Chem. A **116**, 11388 (2012).
[17] L. Halonen, Local mode vibrations in polyatomic molecules, in *Advances in Chemical Physics*, Vol. 104, edited by I. Prigogine and S. A. Rice (John Wiley & Sons, Inc., Hoboken, NJ, USA, 1998).
[18] B. T. Darling and D. M. Dennison, Phys. Rev. **57**, 128 (1940).
[19] G. Herzberg and K.-P. Huber, *Molecular Spectra and Molecular Structure: Constants of Diatomic Molecules* (Van Nostrand Reinhold, New York, 1979), p. 716.
[20] M. E. Kellman, Annu. Rev. Phys. Chem. **46**, 395 (1995).
[21] M. E. Kellman and V. Tyng, Acc. Chem. Res. **40**, 243 (2007).
[22] L. Weinhardt, A. Benkert, F. Meyer, M. Blum, R. G. Wilks, W. Yang, M. Bär, F. Reinert, and C. Heske, J. Chem. Phys. **136**, 144311 (2012).
[23] M. N. Piancastelli, A. Hempelmann, F. Heiser, O. Gessner, A. Rüdel, and U. Becker, Phys. Rev. A **59**, 300 (1999).
[24] A. Hiraya *et al.*, Phys. Rev. A **63**, 042705 (2001).
[25] P. A. Malmqvist, A. Rendell, and B. O. Roos, J. Phys. Chem. **94**, 5477 (1990).
[26] F. Aquilante *et al.*, J. Comp. Chem. **31**, 224 (2010).
[27] Y. Hikosaka, Y. Velkov, E. Shigemasa, T. Kaneyasu, Y. Tamenori, J. Liu, and F. Gel'mukhanov, Phys. Rev. Lett. **101**, 073001 (2008).
[28] F. Gel'Mukhanov, L. Mazalov, and A. Kondratenko, Chem. Phys. Lett. **46**, 133 (1977).
[29] R. Schinke, *Photodissociation Dynamics: Spectroscopy and Fragmentation of Small Polyatomic Molecules, Cambridge Monographs on Atomic, Molecular and Chemical Physics* (Cambridge University Press, Cambridge, 1995).

[30] V. Kimberg, A. Lindblad, J. Söderström, O. Travnikova, C. Nicolas, Y. P. Sun, F. Gelmukhanov, N. Kosugi, and C. Miron, Phys. Rev. X **3**, 011017 (2013).
[31] V. Kimberg and C. Miron, J. Electron. Spectrosc. Relat. Phenom. **195**, 301 (2014).
[32] F. Gelmukhanov and H. Ågren, Phys. Rev. A **54**, 379 (1996).
[33] N. Ignatova, V. V. Cruz, R. C. Couto, E. Ertan, A. Zimin, F. F. Guimarães, S. Polyutov, H. Ågren, V. Kimberg, M. Odelius, and F. Gel'mukhanov, Sci. Rep. **7**, 43891 (2017).
[34] C. Miron, C. Nicolas, O. Travnikova, P. Morin, Y. Sun, F. Gel'mukhanov, N. Kosugi, and V. Kimberg, Nat. Phys. **8**, 135 (2012).
[35] A. Pietzsch *et al.*, Phys. Rev. Lett. **106**, 153004 (2011).
[36] S. Eckert, V. V. da Cruz, R. C. Couto, E. Ertan, F. Fondell, M. Dantz, B. O'Cinneide, T. Schmitt, A. Pietzsch, F. F. Guimarães, H. Ågren, F. Gel'mukhanov, M. Odelius, V. Kimberg, and A. Föhlisch (unpublished).